Role of bulk viscosity in deuteron production in ultrarelativistic nuclear collisions

D. Everett,[1] D. Oliinychenko,[2,3] M. Luzum,[4] J.-F. Paquet,[5,6,7] G. Vujanovic,[8,9] S. A. Bass,[7] L. Du,[10] C. Gale,[10] M. Heffernan,[10] U. Heinz,[1] L. Kasper,[5] W. Ke,[11,12,3] D. Liyanage,[1] A. Majumder,[8] A. Mankolli,[5] C. Shen,[8,13] D. Soeder,[7] J. Velkovska,[5] A. Angerami,[14] R. Arora,[15] S. Cao,[16] Y. Chen,[17,18] T. Dai,[7] R. Ehlers,[19,20,12,3] H. Elfner,[21,22,23] W. Fan,[7] R. J. Fries,[24,25] F. Garza,[24,25] Y. He,[26,27,28] B. V. Jacak,[12,3] P. M. Jacobs,[12,3] S. Jeon,[10] M. Kelsey,[8] M. Kordell, II,[24,25] A. Kumar,[10,8] J. Latessa,[29] Y.-J. Lee,[17,18] A. Lopez,[4] S. Mak,[30] C. Martin,[19] H. Mehryar,[29] T. Mengel,[19] J. Mulligan,[12,3] C. Nattrass,[19] J. H. Putschke,[8] G. Roland,[17,18] B. Schenke,[31] L. Schwiebert,[29] A. Silva,[19] C. Sirimanna,[8] R. A. Soltz,[8,14] J. Staudenmaier,[21] M. Strickland,[32] Y. Tachibana,[33] X.-N. Wang,[12,3] and R. L. Wolpert[30]
(JETSCAPE Collaboration)

[1]*Department of Physics, The Ohio State University, Columbus, Ohio 43210, USA*
[2]*Institute for Nuclear Theory, Department of Physics, University of Washington, Seattle, Washington 98195, USA*
[3]*Nuclear Science Division, Lawrence Berkeley National Laboratory, Berkeley, California 94270, USA*
[4]*Instituto de Fìsica, Universidade de São Paulo, C.P. 66318, 05315-970 São Paulo, São Paulo, Brazil*
[5]*Department of Physics and Astronomy, Vanderbilt University, Nashville, Tennessee 37235, USA*
[6]*Department of Mathematics, Vanderbilt University, Nashville, Tennessee 37235, USA*
[7]*Department of Physics, Duke University, Durham, North Carolina 27708, USA*
[8]*Department of Physics and Astronomy, Wayne State University, Detroit, Michigan 48201, USA*
[9]*Department of Physics, University of Regina, Regina, Saskatchewan S4S 0A2, Canada*
[10]*Department of Physics, McGill University, Montréal, Québec H3A 2T8, Canada*
[11]*Los Alamos National Laboratory, Theoretical Division, Los Alamos, New Mexico 87545, USA*
[12]*Department of Physics, University of California, Berkeley, California 94270, USA*
[13]*RIKEN BNL Research Center, Brookhaven National Laboratory, Upton, New York 11973, USA*
[14]*Lawrence Livermore National Laboratory, Livermore, California 94550, USA*
[15]*Research Computing Group, University Technology Solutions, The University of Texas at San Antonio, San Antonio, Texas 78249, USA*
[16]*Institute of Frontier and Interdisciplinary Science, Shandong University, Qingdao, Shandong 266237, China*
[17]*Laboratory for Nuclear Science, Massachusetts Institute of Technology, Cambridge, Massachusetts 02139, USA*
[18]*Department of Physics, Massachusetts Institute of Technology, Cambridge, Massachusetts 02139, USA*
[19]*Department of Physics and Astronomy, University of Tennessee, Knoxville, Tennessee 37996, USA*
[20]*Physics Division, Oak Ridge National Laboratory, Oak Ridge, Tennessee 37830, USA*
[21]*GSI Helmholtzzentrum für Schwerionenforschung, 64291 Darmstadt, Germany*
[22]*Institute for Theoretical Physics, Goethe University, 60438 Frankfurt am Main, Germany*
[23]*Frankfurt Institute for Advanced Studies, 60438 Frankfurt am Main, Germany*
[24]*Cyclotron Institute, Texas A&M University, College Station, Texas 77843, USA*
[25]*Department of Physics and Astronomy, Texas A&M University, College Station, Texas 77843, USA*
[26]*Key Laboratory of Quark and Lepton Physics (MOE) and Institute of Particle Physics, Central China Normal University, Wuhan 430079, China*
[27]*Guangdong Provincial Key Laboratory of Nuclear Science, Institute of Quantum Matter, South China Normal University, Guangzhou 510006, China*
[28]*Guangdong-Hong Kong Joint Laboratory of Quantum Matter, Southern Nuclear Science Computing Center, South China Normal University, Guangzhou 510006, China*
[29]*Department of Computer Science, Wayne State University, Detroit, Michigan 48202, USA*
[30]*Department of Statistical Science, Duke University, Durham, North Carolina 27708, USA*
[31]*Physics Department, Brookhaven National Laboratory, Upton, New York 11973, USA*
[32]*Department of Physics, Kent State University, Kent, Ohio 44242, USA*
[33]*Akita International University, Yuwa, Akita-city 010-1292, Japan*

(Received 26 March 2022; accepted 7 October 2022; published 5 December 2022)

We use a Bayesian-calibrated multistage viscous hydrodynamic model to explore deuteron yield, mean transverse momentum and flow observables in Pb-Pb collisions at the Large Hadron Collider. We explore theoretical uncertainty in the production of deuterons, including (i) the contribution of thermal deuterons, (ii) models for the subsequent formation of deuterons (hadronic transport vs coalescence), and (iii) the overall

sensitivity of the results to the hydrodynamic model, in particular to bulk viscosity, which is often neglected in studies of deuteron production. Using physical parameters set by a comparison to only light hadron observables, we find good agreement with measurements of the mean transverse momentum $\langle p_T \rangle$ and elliptic flow v_2 of deuterons; however, tension is observed with experimental data for the deuteron multiplicity in central collisions. The results are found to be sensitive to each of the mentioned theoretical uncertainties, with a particular sensitivity to bulk viscosity, indicating that the latter is an important ingredient for an accurate treatment of deuteron production.

DOI: 10.1103/PhysRevC.106.064901

I. INTRODUCTION

Ultrarelativistic ion collisions produce a hot strongly coupled plasma of quarks and gluons which expands, cools down, and recombines into pions, nucleons, other hadrons, and light nuclei. The recent measurements of deuterons, ^{3}He, ^{4}He, and $^3_\Lambda$H at the Large Hadron Collider (LHC) in Pb-Pb collisions at $\sqrt{s_{NN}} = 2.76$ and 5.02 TeV [1–4] have renewed interest in the mechanisms of light nucleus production. The improved precision of measurements provides an opportunity to revisit and test current models of deuteron production.

Three broad types of models are typically used to calculate the production of deuterons in such collisions. The thermal model assumes that light nuclei reach equilibrium with hadrons, until a point of chemical freeze-out, where hadron and nuclear abundances are frozen, which happens at approximately the same temperature across the entire system [5]. To obtain a momentum distribution for the light nuclei, one can combine the thermal model with a blast wave model at a later *kinetic* freeze-out [6]. Another approach is the coalescence model, which predicts that the number of produced light nuclei is a convolution of (i) a source function characterizing the nucleons' distribution in phase space and (ii) the light nucleus's Wigner function.[1] Realistic source functions (space-time-momentum distributions) for the final hadrons can be obtained from hydrodynamics and transport models of heavy-ion collisions. The main assumption of the coalescence model is that light nuclei are formed when hadronic interactions cease. Finally, one can model the production of light nuclei with a transport approach which implements specific production and dissociation reactions—for example $Npn \leftrightarrow Nd$, $\pi pn \leftrightarrow \pi d$, or $\pi d \leftrightarrow pn$ [12–16] (N denotes either p or n)—or binding of nucleons in transport by potentials [17,18].

Ultrarelativistic heavy-ion collisions are frequently simulated by multistage approaches, where the evolution of the plasma is modeled by relativistic viscous hydrodynamics, and the subsequent hadronic rescattering at a more dilute stage is described by kinetic theory. Conveniently, in a multistage simulation, one can test all three types of light nucleus production models. One can sample light nuclei from a near-equilibrium distribution at the transition from hydrodynamics to transport, similarly to a thermal model at chemical freeze-out; one can include the reactions involving deuterons into the transport phase; or one can use the final state nucleons as a source function for coalescence.

In all of these models of light nucleus production, there is a close connection between the distribution of nucleons and the light nucleus bound states that they form. Therefore, it is evident that a successful description of light nuclei relies on a good description of the underlying system evolution.

To test the above light nucleus production models, we employ a hybrid hydrodynamic and hadronic transport model that was calibrated to a wide set of hadron observables [19,20]. Importantly, this multistage model includes bulk viscosity, unlike most previous studies of light nuclei. While uncertainties remain in the magnitude of bulk viscosity of QCD, and in particular the modeling of its effect on particlization, it is generically expected to have a larger effect on heavier particles, and therefore should be important for the production of light nuclei. We show in this work that bulk viscosity indeed has a large effect on deuteron production, regardless of the underlying deuteron production model.

This work is organized as follows. In Sec. II, we first briefly describe our multistage hydrodynamic model and deuteron production models used in this work. We then compare the multistage model with measured deuteron observables—yield dN/dy, mean transverse momenta $\langle p_T \rangle$, and azimuthal angular anisotropy v_2—in Pb-Pb at the LHC in Secs. III A and III B. We further quantify via Bayesian inference the additional constraints provided by deuteron observables on the initial conditions and bulk viscosity of the plasma in Sec. III C, and summarize our results in Sec. IV.

II. MODEL OVERVIEW

A. Multistage model of heavy ion collisions

A detailed description of the hybrid hydrodynamic-transport model used throughout this work can be found in Ref. [20]. Briefly, the T$_\mathrm{R}$ENTo model [21] is used as a parametric initialization for the energy density shortly after the impact of the nuclei. This profile is then free streamed for a short proper time, and is then used as initialization for second-order relativistic viscous hydrodynamics (MUSIC [22–24]). We use the shear and bulk viscosity parametrizations described in Refs. [19,20] and an equation of state which matches the trace anomaly of lattice calculations [25] and the hadron resonance gas. On a surface of constant temperature T_sw, the Cooper-Frye prescription [26] is employed to switch the description ("particlization") from fluid to a kinetic theory of hadrons,

[1] Although the quantum mechanical foundations of the coalescence model have been studied for many years [7–10], modern implementations can still vary substantially both in methods and results, especially for nuclei heavier than the deuteron. Different types of coalescence models are listed, for example, in Ref. [11]. We will use a model where nucleons from transport, free-streamed to the larger of their last interaction times, are convoluted with a Gaussian deuteron Wigner function in their center-of-mass frame; see Sec. II C.

TABLE I. Model parameters used to produce the predictions in this work. See Refs. [19,20] for details.

Parameter	Value	Parameter	Value	Parameter	Value
N(2.76 TeV) (GeV)	14.2	τ_R (fm/c)	1.48	$(\zeta/s)_{\max}$	0.13
N(5.02 TeV) (GeV)	18.8	α	0.047	$T_{\zeta,c}$ (GeV)	0.12
$T_{\eta,\mathrm{kink}}$ (GeV)	0.22	p	0.06	w_ζ (GeV)	0.089
$a_{\eta,\mathrm{low}}$ (GeV^{-1})	−0.76	k	0.98	λ_ζ	−0.19
$a_{\eta,\mathrm{high}}$ (GeV^{-1})	0.22	w (fm)	1.12	b_π	4.5
$(\eta/s)_{\mathrm{kink}}$	0.096	d^3_{min} (fm^3)	2.97	T_{sw} (GeV)	0.136

which then scatter, decay, and form resonances in the SMASH hadronic afterburner [27–29].

In the ideal hydrodynamic limit, as in the case of thermal models, the hadrons in the fluid are in local equilibrium. In kinetic theory, it implies that their momentum distribution is given by the Bose-Einstein or Fermi-Dirac distribution. In the more general case where there is dissipation in hydrodynamics, there is an off-equilibrium correction to the hadron distribution, and this viscous correction is model dependent [30–32]. In this work, we use the "Grad" model [33] for viscous corrections to the equilibrium distribution function, the one out of several studied in Refs. [19,20] that gave the best agreement with light hadron measurements (listed below).

The model parameters were calibrated by Bayesian parameter estimation against observables for Pb-Pb collisions at $\sqrt{s_{NN}} = 2.76$ TeV as well as Au-Au collisions at $\sqrt{s_{NN}} = 0.2$ TeV. The Pb-Pb observables include the yields and mean transverse momenta of pions, kaons, and protons [34], the charged particle multiplicity and transverse energy [35,36], the charged particle elliptic, triangular, and quadrangular flow [37], and the charged particle mean transverse momentum fluctuations [38]. The calibration observables for Au-Au collisions include the yields and mean transverse momenta of pions and kaons [39] and the charged particle elliptic and triangular flow [40,41]. In particular, no deuteron or light nuclei measurements were used in the calibration of these parameters. The parameters used to generate the predictions in the next section are listed in Table I.[2]

We explore several different models of deuteron production, including sampling on the switching hypersurface, production via three-body scattering in the hadronic afterburner, and coalescence on the kinetic freeze-out surface.

B. Deuteron production with transport

We investigate two models of deuteron production with transport:

(i) "Transport only," which assumes that no deuterons are present at the transition from hydrodynamics to hadronic transport (i.e., at "particlization"); rather, all deuterons are created during the hadronic rescattering phase by reactions $\pi d \leftrightarrow \pi np$, $Nd \leftrightarrow Nnp$, $\bar{N}d \leftrightarrow \bar{N}np$, and $\pi d \leftrightarrow NN$; and all of their CPT conjugates, with elastic πd, Nd, and $\bar{N}d$ also changing the deuterons' momenta.

(ii) "Cooper-Frye + transport," which assumes that deuterons are nearly equilibrated with the hadron resonance gas at the transition from hydrodynamics, so that they are sampled according to near-equilibrium distribution functions and subsequently allowed to be formed and/or destroyed in the hadronic rescattering phase.

Notice that the yield of deuterons at the Cooper-Frye sampling in the model (ii) is closely related to the results of a thermal model (discussed in the introduction) with freeze-out temperature T_{sw} and volume $V = \int d\sigma_\mu u^\mu$, where $d\sigma_\mu$ are the normal four-vectors to the hypersurface, and u^μ are the collective velocities of the hypersurface elements. These quantities enter the Cooper-Frye formula [26]

$$P^0 \frac{dN}{d^3p} = \frac{g}{(2\pi\hbar)^3} \int d\sigma_\mu P^\mu (f_{eq}(P_\nu u^\nu/T) + \delta f), \quad (1)$$

with $f(P_\nu u^\nu/T)$ for deuterons being the Bose-Einstein distribution, δf being a correction due to viscosity, and g their degeneracy factor. Typically, thermal models assume local equilibrium, $\delta f = 0$.

In this work we use the implementation of these $3 \to 2$ reactions via an intermediate fictitious d' resonance [14]: $pn \leftrightarrow d'$, $\pi d' \leftrightarrow \pi d$, $Nd' \leftrightarrow Nd$. Recently a possibility to simulate $3 \to 2$ reactions directly, without d', via stochastic rates was implemented in SMASH [42], but it is not employed in this work. In Ref. [42] it was shown that the main difference between direct $3 \to 2$ reactions and reactions with the intermediate d' resonance is that $3 \to 2$ reactions bring the deuteron yield to equilibrium faster.

C. Deuteron production with coalescence

Here we employ a Wigner-function coalescence model [9] that has no free parameters. The implementation of coalescence is based on the equation

$$\frac{d^3N_d}{d^3\boldsymbol{p}_d} = \frac{3}{8} \int \frac{d^3\boldsymbol{r}_d d^3\boldsymbol{r} d^3\boldsymbol{q}}{(2\pi\hbar)^6} \mathcal{D}(\boldsymbol{r},\boldsymbol{q}) \times W\left(\frac{\boldsymbol{p}_d}{2}+\boldsymbol{q}, \frac{\boldsymbol{p}_d}{2}-\boldsymbol{q}, \boldsymbol{r}_d+\frac{\boldsymbol{r}}{2}, \boldsymbol{r}_d-\frac{\boldsymbol{r}}{2}\right), \quad (2)$$

[2]The parameters in Table I are slightly different from the maximum *a posteriori* parameters reported in Refs. [19,20], but remain parameters of high posterior probability density. The multidimensional posterior does not have a very sharply defined global maximum, and the maximum *a posteriori* parameters can differ slightly depending on the details of the Markov chain Monte Carlo optimization.

where the factor 3/8 originates from spin and isospin averaging. The deuteron Wigner function is $\mathcal{D}(\boldsymbol{r},\boldsymbol{q}) = 8\exp(-|\boldsymbol{r}|^2/d^2 - |\boldsymbol{q}|^2 d^2/\hbar^2)$, which originates from

$$\mathcal{D}(\boldsymbol{r},\boldsymbol{q}) = \int d^3\boldsymbol{\xi} e^{i\boldsymbol{q}\cdot\boldsymbol{\xi}/\hbar}\varphi_d(\boldsymbol{r}+\boldsymbol{\xi}/2)\varphi_d^*(\boldsymbol{r}-\boldsymbol{\xi}/2), \quad (3)$$

where the deuteron wave function φ_d is assumed to be a Gaussian with $d = 3.2$ fm [43]. The function W is the probabilityof finding a pair of nucleons at positions $\boldsymbol{r}_d \pm \boldsymbol{r}/2$ with momenta $\boldsymbol{p}_d/2 \pm \boldsymbol{q}$. In our model the distribution W is represented by the nucleon pairs in the hadronic afterburner. The integrals in Eq. (2) are computed as a sum over all nucleon pairs in the simulation. Every pair is transported in time to the latest of their last collision times. At this moment $\boldsymbol{r}_1, \boldsymbol{r}_2$ are coordinates and $\boldsymbol{p}_1$ and $\boldsymbol{p}_2$ are momenta of the nucleons. Then

$$\boldsymbol{r}_d = \tfrac{1}{2}(\boldsymbol{r}_1 + \boldsymbol{r}_2), \quad \boldsymbol{r} = \boldsymbol{r}_1 - \boldsymbol{r}_2, \quad (4)$$

$$\boldsymbol{p}_d = \boldsymbol{p}_1 + \boldsymbol{p}_2, \quad \boldsymbol{q} = \tfrac{1}{2}(\boldsymbol{p}_1 - \boldsymbol{p}_2), \quad (5)$$

and the pair contributes to deuteron spectra with the weight $\frac{3}{8}\mathcal{D}(\boldsymbol{r},\boldsymbol{q})$.

III. RESULTS

A. Comparing transport, coalescence, and thermal-like deuteron production

To investigate the different mechanisms of deuteron production, we compare the three specific scenarios presented in Secs. II B and II C within our multistage model of heavy ion collisions:

(i) Transport only: Deuterons not present at particlization, followed by hadronic transport with deuteron reactions.
(ii) Cooper-Frye + transport: Deuterons present at particlization and allowed to react in the hadronic transport.
(iii) Coalescence only: Deuterons not present at particlization, hadronic transport without deuteron reactions, followed by coalescence at kinetic freeze-out.

While these do not represent all possible variations, they provide sufficient information for understanding the effects of each mechanism.

In Fig. 1 one can see that these three scenarios result in rather similar yield and mean transverse momentum of deuterons. Let us concentrate on the comparison of the transport scenarios first. As in previous studies [14,15], deuteron yields and average transverse momenta are similar whether or not deuterons are sampled at particlization. To understand this effect, note that (i) the reaction $\pi d \to \pi pn$ has a large cross section, (ii) the implementation of the reverse reaction obeys the detailed balance principle, and (iii) a large number of pions is produced in heavy ion collisions. Given these conditions, as long as the $\pi d \leftrightarrow \pi pn$ reaction rate is larger than the expansion rate of the plasma, deuterons rapidly approach relative equilibrium with protons. When the deuteron is not sampled at particlization, the deuteron yield approaches but does not completely reach equilibrium [14,15], because the fireball's expansion freezes out the $\pi d \leftrightarrow \pi pn$ reactions; this is the

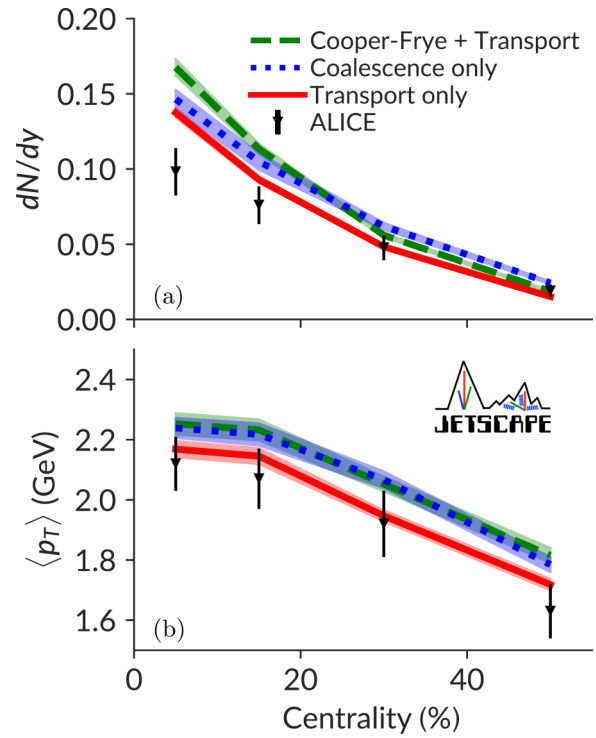

FIG. 1. Comparison of the deuteron midrapidity yield (a) and mean transverse momentum (b) in $\sqrt{s_{NN}} = 2.76$ TeV Pb-Pb collisions for three scenarios of deuteron production. The bands represent the statistical uncertainty on the calculations. Experimental data from Ref. [1]. See text for more details.

reason for the slightly smaller number of deuterons found in the "transport only" scenario. Note that, to avoid confusion, one should think about deuterons being in equilibrium in a statistical sense, averaging over a large number of heavy-ion collisions, and not in a single event; notice that on average only around 0.1 deuterons are produced per event per unit of rapidity, as shown in Fig. 1.

In Refs. [14,15] both scenarios (i) and (ii) were found to be compatible with the experimental data, although sampling deuterons at particlization was slightly preferred. In this work, the situation is different: the experimentally measured deuteron yield and transverse momentum are better described by omitting the deuteron from particlization (see Fig. 1). While there are multiple differences between the multistage models used in the present work and Refs. [14,15], the likely reason for this difference is bulk viscosity, which was not included in previous works. We discuss this effect in detail in Sec. III C. We note that the (mostly systematic) uncertainties are still significant on the deuteron measurements [1] shown in Fig. 1. Reduction of these systematic uncertainties would increase the discrimination power of deuterons even further.

The creation of deuterons by reactions has a certain similarity to coalescence. With reactions, most of final-state deuterons are produced rather late; earlier produced deuterons tend to get destroyed by subsequent collisions. Moreover, by the kinematics of the $\pi pn \to \pi d$ reaction, the incoming proton and neutron have to be close in phase space, as coalescence assumes. In Fig. 1 one can indeed see that the

coalescence model provides a very similar deuteron yield and transverse momentum as the models with deuteron-producing reactions. Therefore, it is the underlying proton phase space distribution (which is the same in all three models) that influences the deuteron observables here, while the deuteron production mechanism is less important.[3] As a consequence, the model parameters that influence proton production will also influence deuteron production. This means that by combining proton and deuteron observables one could potentially constrain these parameters better than by using only proton observables.

Based on the agreement of model predictions with measured proton data, one might expect a better agreement for deuteron yields. There are several reasons why the deuteron yield is not as well described as expected. First, although the model is tuned to describe integrated proton yield and $\langle p_T \rangle$ precisely, the proton p_T spectrum in fact exhibits deviations from experiment [[20], Fig. 17]. Second, previous studies suggesting that a good agreement of proton data implies good agreement with deuteron data [14,15] did not take into account bulk viscosity, unlike in the present work. Importantly, the bulk viscous corrections to the proton p_T spectrum are substantial (see Fig. 4 below).

B. Yield, mean p_T, and flow of deuterons at $\sqrt{s_{NN}} = 5.02$ TeV

In this section we provide a prediction for the multiplicity and mean p_T of deuterons for Pb-Pb $\sqrt{s_{NN}} = 5.02$ TeV collisions using the "Transport only" approach. We further compare our calculation for p_T differential v_2 with ALICE measurements for deuterons in both Pb-Pb $\sqrt{s_{NN}} = 2.76$ TeV and $\sqrt{s_{NN}} = 5.02$ TeV.

The initial conditions, transport coefficients, and other parameters of the multistage model given in Table I were not calibrated using Pb-Pb $\sqrt{s_{NN}} = 5.02$ TeV observables, but to Pb-Pb $\sqrt{s_{NN}} = 2.76$ TeV and Au-Au $\sqrt{s_{NN}} = 0.2$ TeV observables [19,20]. We assume that all model parameters remain the same except for two T$_\mathrm{R}$ENTo initial condition parameters that are expected to be center-of-mass energy dependent: (i) the nucleon-nucleon inelastic cross section and (ii) the overall normalization of the initial energy density. For the inelastic nucleon-nucleon cross section at $\sqrt{s_{NN}} = 5.02$ TeV, we used 70 mb. The normalization of the initial energy density is typically a parameter tuned to heavy ion measurements, mostly the hadronic multiplicities. In our approach, instead of retuning it to measurements, we simply estimated it from a previous Bayesian inference that also used T$_\mathrm{R}$ENTo initial condition [44]. In that work, they found the ratio of the normalization[4] at $\sqrt{s_{NN}} = 5.02$ TeV and $\sqrt{s_{NN}} = 2.76$ TeV to be 1.32, yielding the normalization value at $\sqrt{s_{NN}} = 5.02$ TeV quoted in Table I.

The comparison with measurements from ALICE [45–47] is shown in Fig. 2. The agreement between the calculations

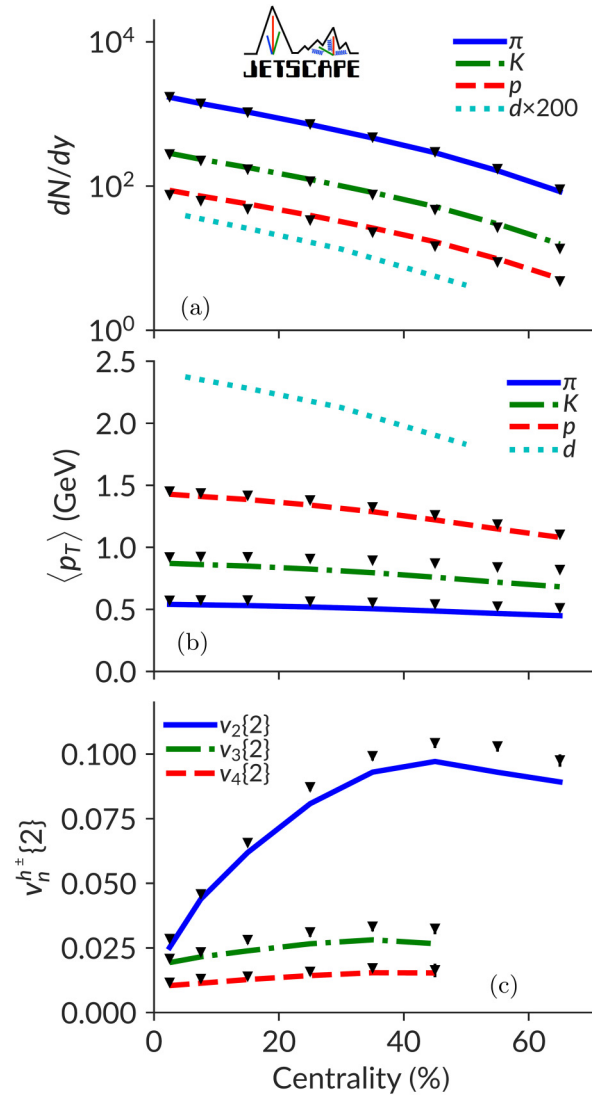

FIG. 2. Model predictions for Pb-Pb $\sqrt{s_{NN}} = 5.02$ TeV collisions with parameters given in Table I. The model was calibrated only to Pb-Pb $\sqrt{s_{NN}} = 2.76$ TeV and Au-Au $\sqrt{s_{NN}} = 0.2$ TeV observables. The deuteron was not sampled on the switching surface, but only allowed to form during the SMASH hadronic cascade (the "transport only" scenario). ALICE measurements [45–47] are plotted as black triangles.

and hadron measurements is very similar to that found at $\sqrt{s_{NN}} = 2.76$ TeV; see Ref. [[20], Fig. 8]. Our prediction for the deuteron multiplicity and mean p_T at $\sqrt{s_{NN}} = 5.02$ TeV is shown on the same figure. As is the case for light hadrons, it is natural to expect our predictions for deuterons at 5.02 TeV to have very similar agreement as for the 2.76 GeV results (see the "transport only" curve in Fig. 1); that is, generally good agreement except for an overestimated yield in central collisions.

The p_T differential v_2 of deuterons in Pb-Pb collisions at $\sqrt{s_{NN}} = 2.76$ TeV and 5.02 TeV is described very well for different collision centralities, as shown in Fig. 3. The $\sqrt{s_{NN}} = 5.02$ TeV v_2 result was shown as a prediction in the ALICE publication [4]. We evaluate the p_T-differential

[3]This may be different in small systems where the span of the deuteron wave function is comparable to the system size.

[4]More specifically, these are the normalizations for the maximum *a posteriori* parameters of each system.

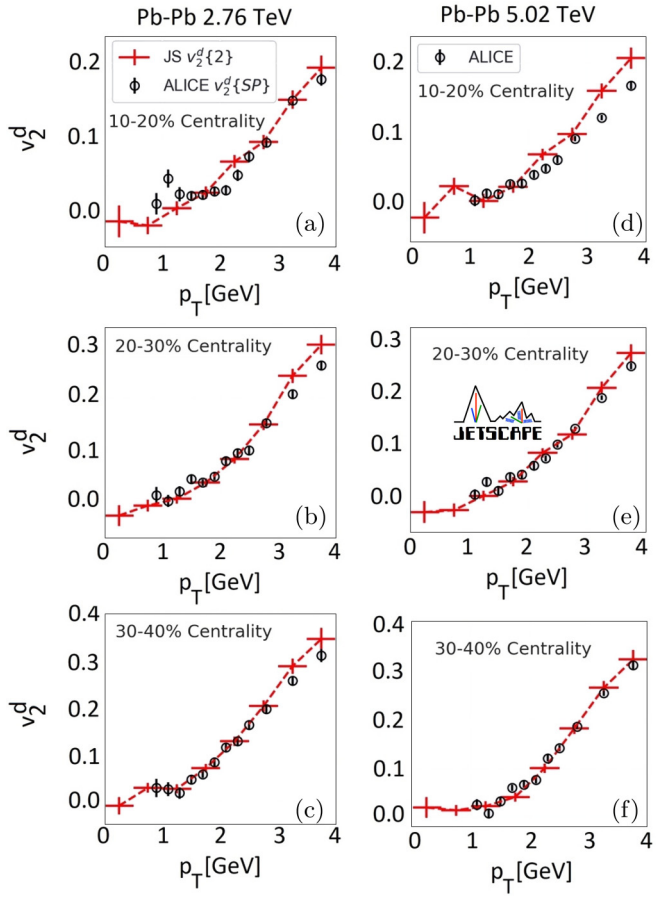

FIG. 3. The differential v_2 for deuterons for three centrality bins for Pb-Pb collisions at 2.76 TeV (a)–(c) and 5.02 TeV (d)–(f). Our calculations for the "transport only" approach are red crosses, and ALICE measurements [4] are black circles. The model observables are averaged over 5000 fluctuating initial conditions.

deuteron momentum anisotropy $v_2\{2\}$ using the Q-cumulant method [48].

C. Sensitivity to medium properties

In this section, we explore the sensitivity of the deuteron yield and mean transverse momentum to properties of the hydrodynamic medium.

As discussed in Sec. II, deviations of the plasma from local thermal equilibrium lead to modifications in the corresponding hadronic momentum distribution from Bose-Einstein or Fermi-Dirac. This "viscous correction" to the equilibrium distribution function is related to the magnitude of the bulk pressure. Its dependence on the hadron mass depends on the model used to calculate the viscous corrections. For the Grad model used in this work, this viscous correction increases with the hadron mass.[5] As a result, heavy particles such as protons, neutrons, and especially deuterons might be expected

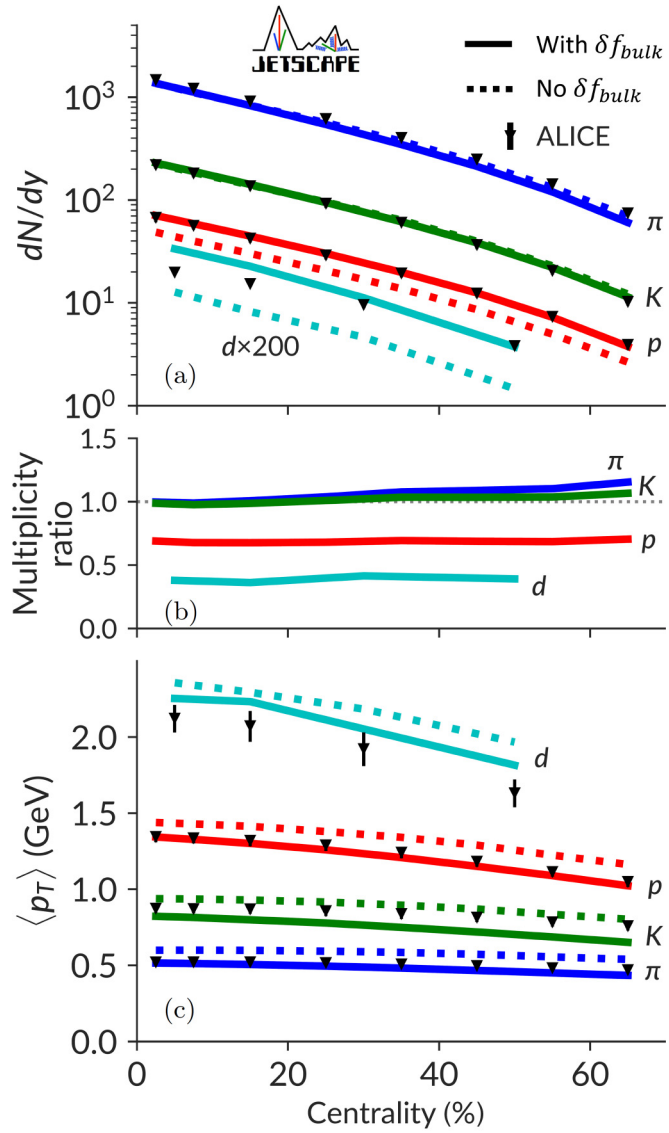

FIG. 4. Identified hadron multiplicity (a) and mean p_T (c) for Pb-Pb $\sqrt{s_{NN}} = 2.76$ TeV as a function of centrality, with (solid line) or without (dotted line) the bulk viscous correction δf_{bulk} in Cooper-Frye for all particles. The ratio of of multiplicity without and with bulk corrections at particlization are shown in panel (b). Deuterons are produced at particlization and allowed to dynamically form and be destroyed, corresponding to the "Cooper-Frye+transport" scenario discussed in Sec. III A. Note that the effect of the viscous correction on pions, protons and other hadrons propagate to deuterons through the transport phase. ALICE measurements [1,34] are plotted as black triangles.

to have a higher sensitivity to bulk viscosity, compared to the majority of produced hadrons. Despite this, there has been no systematic study of the role of bulk viscosity in the production of deuterons until now.

In Fig. 4, we investigate the relative importance of bulk viscosity by comparing the yield of each particle (solid line) to the case where the bulk viscous correction at particlization has been set by hand to zero for all particles (dotted line). One can see that the importance of the viscous correction indeed

[5]We note that systematic studies of the mass dependence of bulk viscous corrections, and their effect on light nuclei production, could help differentiate between different models of viscous corrections.

TABLE II. Range of model parameters used to produce the model predictions in this section. Note that the highest bulk viscosity to entropy ratio ζ/s attained in the fluid before switching (at temperature $T_{\rm sw} = 0.136$ GeV) lies in the range $0.029 \lesssim (\zeta/s)(T_{\rm sw}) \lesssim 0.143$; this is slightly smaller than the nominal maximum value $(\zeta/s)_{\rm max}$ defined at temperature $T_{\zeta,c} = 0.12$ GeV (see Table I for the values of the model parameters).

Parameter	Minimum	Maximum
$(\zeta/s)_{\rm max}$	0.03	0.15
k	0.3	2
w (fm)	0.5	1.5

increases significantly with mass, and that the yield of deuterons is affected much more than that of lighter hadrons; generically the identified hadron multiplicity gets enhanced whereas the mean p_T gets reduced by the bulk viscous correction. Note that, while the distribution of deuterons at particlization does not have a strong effect on the final deuteron distribution (see discussion in Sec. III A), any change in the distribution of protons and pions subsequently feeds down to the deuteron.

To better understand the role of bulk viscosity on deuteron production, we proceed with a Bayesian analysis with three parameters of interest. Two parameters, k and w, enter the initial conditions via the T_RENTo model. The parameter $k \equiv 1/\sigma_k^2$ controls the magnitude of the fluctuations of the deposited energy in each nucleon-nucleon collision. The parameter w, referred to as the nucleon width, controls the transverse radius of the nucleons in T_RENTo, and defines the transverse size of deposited energy given a nucleon-nucleon collision. Both of these parameters largely control the homogeneity of the initially deposited energy density. Finally, we vary the magnitude of the specific bulk viscosity at its peak value, $(\zeta/s)_{\rm max}$. The temperature dependence of bulk viscosity in this work is assumed to have a skewed-Cauchy form as in Ref. [[20], Fig. 1]. The priors for each parameter are assumed to be uniform within the ranges listed in Table II. The range of temperature-dependent specific bulk viscosities spanned by the prior for $(\zeta/s)_{\rm max}$ is shown in Fig. 5. For deuteron production, we use the "coalescence only" model described in Secs. II and III A.

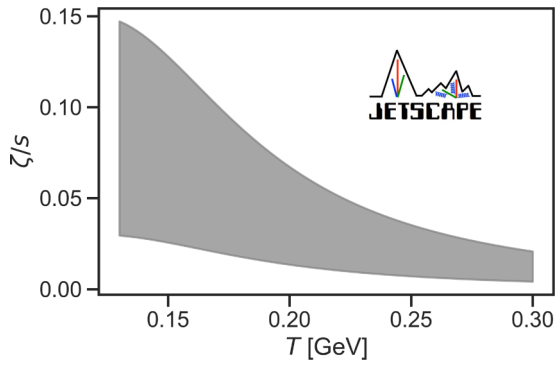

FIG. 5. The allowed range of specific bulk viscosity permitted by the chosen Bayesian prior. Only the magnitude was varied, while the shape parameters were held fixed by the values in Table I.

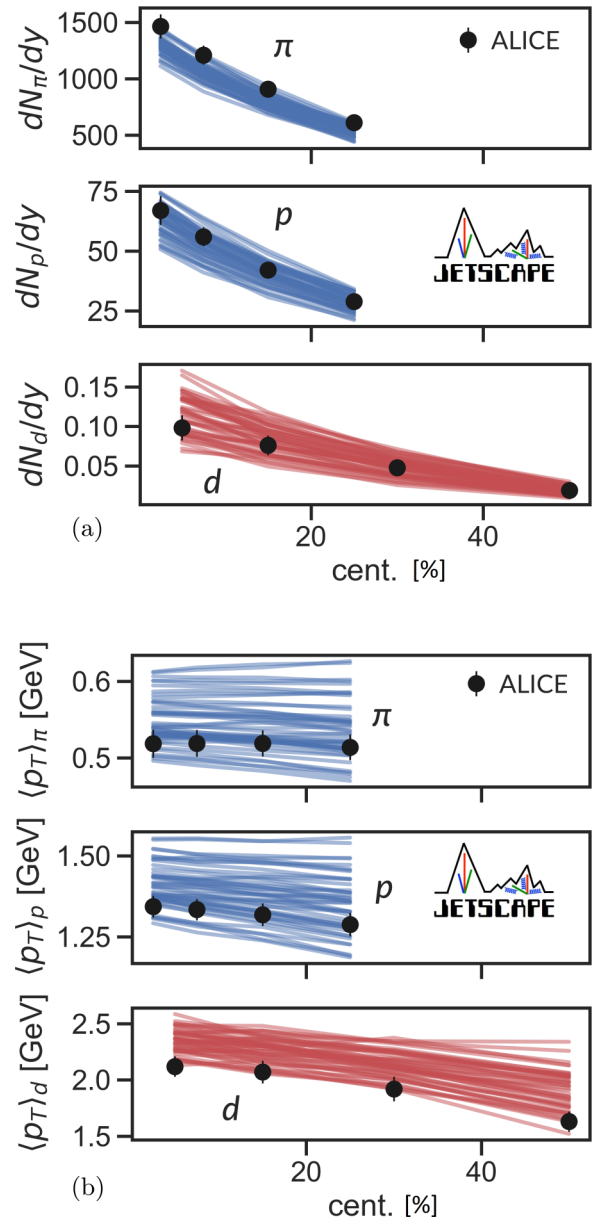

FIG. 6. Prior predictive distributions for the particle yields (a) and mean p_T (b), given by model predictions at the 45 points sampled uniformly in the prior volume. These points form the Gaussian process design. ALICE data are from Refs [1,34].

Forty-five design points were sampled from the prior using a Latin hypercube design [49]. Combined with the fixed values of all remaining model parameters, the model's predictions (given by the model's prior predictive distribution) for these 45 samples of k, w, and $(\zeta/s)_{\rm max}$ are shown in Fig. 6 for the distributions of pion, proton, and deuteron yields and mean p_T in Pb-Pb $\sqrt{s_{NN}} = 2.76$ TeV collisions.

We perform the Bayesian inference along the lines of previous works [19,20,44,50–55]: For each observable, an emulator is used to interpolate the model's results between the parameter point samples. The major difference with previous

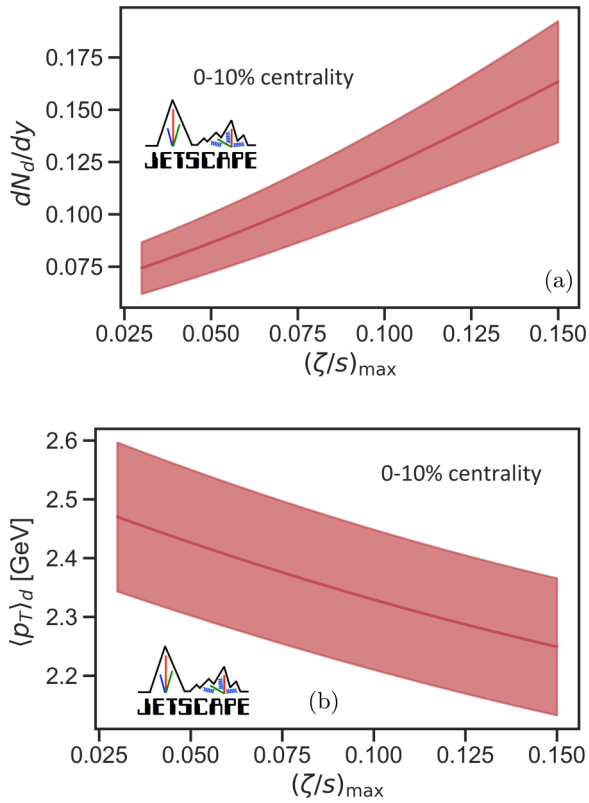

FIG. 7. The response of the deuteron yield dN_d/dy (a) and mean p_T (b) to the change of the magnitude of the specific bulk viscosity $(\zeta/s)_{\max}$, for Pb-Pb $\sqrt{s_{NN}} = 2.76$ TeV 0–10% centrality.

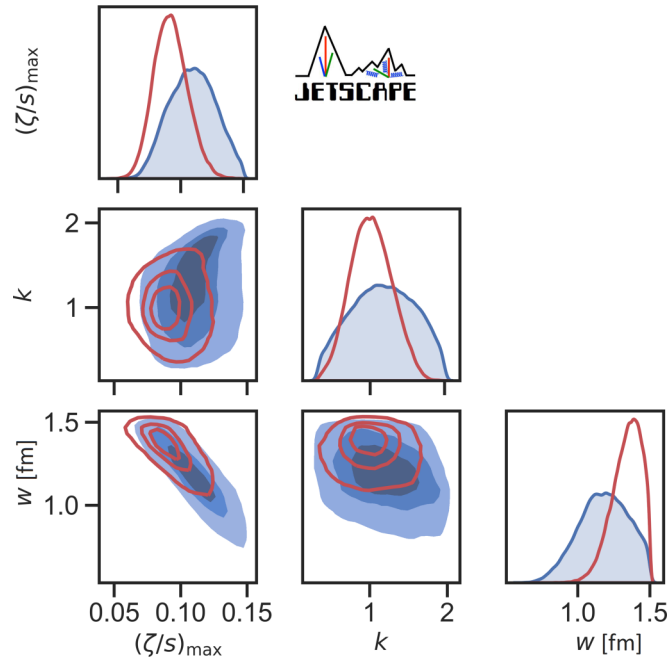

FIG. 8. The posterior density of single (diagonal) and joint (off diagonal) marginal posterior distributions of the three model parameters, calibrated to pion and proton observables (shaded blue) or pion, proton, and deuteron observables (unshaded red).

work is that we use a more sophisticated Gaussian process emulator.[6]

To illustrate the sensitivity of deuteron observables to the magnitude of the bulk viscosity, we fix the T_RENTo fluctuation k and nucleon width w to the midpoints of their prior, and plot the emulated response of the deuteron yield and mean transverse momenta to changes in the specific bulk viscosity $(\zeta/s)_{\max}$. This is shown in Fig. 7, and we see that the deuteron yield indeed shows a strong sensitivity to the magnitude of bulk viscosity; the mean transverse momenta is also found to be sensitive to $(\zeta/s)_{\max}$.

In Fig. 8 we show the effect of adding deuteron observables on constraining the nucleon width w, the fluctuation parameter k, and the maximum of bulk viscosity $(\zeta/s)_{\max}$. We see that the deuteron's dependence on bulk viscosity modifies the value of $(\zeta/s)(T)$ that is in best agreement with measurements. Moreover, Fig. 8 shows how this change in bulk viscosity correlates with changes in the preferred value of the initial condition parameters. For example, we see that including deuteron observables would favor a slightly smaller $(\zeta/s)_{\max}$ and a larger w; the former can be understood from the fact that simulations with parameters calibrated without deuteron observables overestimate the deuteron multiplicity [see Fig. 1(a)] whereas decreasing $(\zeta/s)_{\max}$ helps to reduce the tension (see Fig. 7), and the latter can be understood by its anticorrelation with w. We do not intend these results to represent accurate calibrations of the three model parameters considered here, in part because we only explored a small subspace of the much larger parameter space considered in Ref. [20], and in part because we only calibrated the three model parameters against a small set of observables.[7] Nevertheless, Fig. 8 illustrates the sensitivity of deuterons to bulk viscosity and their potential for improving constraints on the properties of quark-gluon plasma.

IV. SUMMARY

We explored deuteron production in ultrarelativistic Pb+Pb collisions at $\sqrt{s_{NN}}$ of 2.76 and 5.02 TeV, two collision

[6]Rather than performing a linear dimensionality reduction of the model outputs, such as principal component analysis, we train a *multitask* Gaussian process regression [56] as the model surrogate. If two observables are labeled by i and j, and two vectors of model parameters labeled by $\boldsymbol{x}$ and $\boldsymbol{x}'$, then the multitask kernel function is given by

$$k_{ij}(\boldsymbol{x}, \boldsymbol{x}') = k(\boldsymbol{x}, \boldsymbol{x}')k_{\text{task}}(i, j),$$

where $k(\boldsymbol{x}, \boldsymbol{x}')$ plays the role of the usual kernel function, and $k_{\text{task}}(i, j)$ is a kernel function which models the correlations among different outputs.

[7]In particular, differences between Fig. 8 and the results in Ref. [20] are not necessarily from the addition of deuteron observables: the smaller space of parameter that is varied, as well as the smaller number of observables used to produce Fig. 8, also modify correlations in the parameter posterior.

systems where recent deuteron measurements are available. For this purpose we employed a multistage approach (hydrodynamics + hadronic afterburner) tuned to reproduce the yields, mean transverse momenta, and flow of pions, kaons, and protons in Au-Au collisions at $\sqrt{s_{NN}} = 0.2$ TeV and Pb-Pb collisions at $\sqrt{s_{NN}} = 2.76$ TeV; no deuteron observables were used for tuning. Three different models of deuteron production were tested: "transport only," "Cooper-Frye + transport," and "coalescence only" (Sec. III A). Overall, all three models produce rather similar results. At 2.76 TeV they reproduce the centrality dependence of deuteron $\langle p_T \rangle$ and $v_2(p_T)$ within error bars, while the deuteron yields are overestimated in central collisions but reproduced well in more peripheral ones. It is possible that a more realistic deuteron wave function might affect the centrality dependence and lead to improvement in central collisions, but we have not checked this.

Our predictions for deuteron flow at 5.02 TeV was confronted with experimental data in Ref. [4], with good overall agreement. This was expected, since the deuteron flow is not much different at 2.76 and 5.02 TeV and the model reproduced the deuteron $v_2(p_T)$ at 2.76 TeV very well. The data for deuteron yields at 5.02 TeV have not yet been published by ALICE, although, analogously to 2.76 TeV, it would not be surprising that our prediction overestimates the yield in central collisions, reproduces it in peripheral collisions, and reproduces the $\langle p_T \rangle$ precisely. Despite the above tension with 2.76 TeV measurements in central collisions, we expect our prediction for the ratio of measured yields at 5.02 and 2.76 TeV to be more robust.

The main conclusion of this study is that deuteron observables are particularly sensitive to bulk viscosity. We have seen in Fig. 4 that, when bulk viscous corrections change the proton and neutron yield by 20–25%, the deuteron yield can be changed by as much as 50%. While the quantitative values for the bulk viscous corrections quoted above are quite large—and might be even pushing the multistage model to its limits [57–60]—the stronger dependence on bulk viscosity of deuterons compared to protons should be robust.

The fact that deuterons are sensitive to the bulk viscous corrections has an interesting implication: Proton femtoscopic radii should also be sensitive to the bulk viscosity. Indeed, a relation between proton femtoscopic radii and coalescence was explicitly demonstrated recently [10].

The overall dependence of light nuclear observables on bulk viscosity could be used to improve constraints on this transport coefficient, as discussed in Sec. III C. We have provided a preliminary constraint in Fig. 8; a more robust constraint will require a better understanding of the bulk viscosity in heavy ion collisions, in particular viscous corrections at the transition between hydrodynamics and transport.

ACKNOWLEDGMENTS

This work was supported in part by the National Science Foundation (NSF) within the framework of the JETSCAPE Collaboration, under Grant No. OAC-2004571 (CSSI:X-SCAPE). It was also supported under ACI-1550172 (Y.C. and G.R.), ACI-1550221 (R.J.F., F.G., and M.K.), ACI-1550223 (D.E., U.H., L.D., and D.L.), ACI-1550225 (S.A.B., T.D., W.F., and R.W.), ACI-1550228 (R.E., B.J., P.J., J.M., and X.-N.W.), ACI-1550300 (S.C., A.K., A.M., C.N., A.S., J.P., L.S., C.Si., R.A.S., and G.V.), PHY-1516590 and PHY-1812431 (R.J.F., F.G., M.K.), and PHY-2012922 (C.S.); it was supported in part by NSF CSSI Grant No. OAC-2004601 (BAND; D.L. and U.H.); it was supported in part by the U.S. Department of Energy, Office of Science, Office of Nuclear Physics under Grants No. DE-AC02-05CH11231 (X.-N.W.), DE-FG02-00ER41132 (D.O.), DE-AC52-07NA27344 (A.A. and R.A.S.), DE-SC0013460 (S.C., A.K., A.M., C.S., and C.Si.), DE-SC0004286 (L.D., D.E., U.H., and D. L.), DE-FG02-92ER40713 (J.P.), DE-FG02-05ER41367 (T.D., J.-F.P., D.S., and S.A.B.), DE-SC0021969 (C.S.), and DE-FG05-92ER40712 (L.K., A.M., J.V.), and under Contract No. DE-SC0012704 (B.S. and C.S.). The work was also supported in part by the National Science Foundation of China (NSFC) under Grants No. 11935007, 11861131009, and 11890714 (Y.H.), by the Natural Sciences and Engineering Research Council of Canada (C.G., M.H., S.J., and G.V.), by the Office of the Vice President for Research (OVPR) at Wayne State University (Y.T.), by the São Paulo Research Foundation (FAPESP) under Projects 2016/24029-6, 2017/05685-2, 2018/24720-6, and 2021/08465-9 (A.L. and M.L.), and by the University of California, Berkeley – Central China Normal University Collaboration Grant (W.K.). U.H. would like to acknowledge support by the Alexander von Humboldt Foundation through a Humboldt Research Award. C.S. acknowledges support from a DOE Office of Science Early Career Award. Allocation of super-computing resources (Project No. PHY180035) was obtained in part through the Extreme Science and Engineering Discovery Environment (XSEDE), which is supported by National Science Foundation Grant No. ACI-1548562. Calculations were performed in part on Stampede2 compute nodes, generously funded by the National Science Foundation (NSF) through Award No. ACI-1134872, within the Texas Advanced Computing Center (TACC) at the University of Texas at Austin [61], and in part on the Ohio Supercomputer [62] (Project No. PAS0254). Computations were also carried out on the Wayne State Grid funded by the Wayne State OVPR. Data storage was provided in part by the OSIRIS project supported by the National Science Foundation under Grant No. OAC-1541335.

[1] J. Adam *et al.* (ALICE), Production of light nuclei and antinuclei in *pp* and Pb-Pb collisions at energies available at the CERN Large Hadron Collider, Phys. Rev. C **93**, 024917 (2016).

[2] J. Adam *et al.* (ALICE Collaboration), ${}^{3}_{\Lambda}\mathrm{H}$ and ${}^{3}_{\Lambda}\overline{\mathrm{H}}$ production in Pb-Pb collisions at $\sqrt{s_{\mathrm{NN}}} = 2.76$ TeV, Phys. Lett. B **754**, 360 (2016).

[3] S. Acharya *et al.* (ALICE Collaboration), Production of ${}^{4}\mathrm{He}$ and ${}^{4}\overline{\mathrm{He}}$ in Pb-Pb collisions at $\sqrt{s_{\mathrm{NN}}} = 2.76$ TeV at the LHC, Nucl. Phys. A **971**, 1 (2018).

[4] S. Acharya *et al.* (ALICE Collaboration), Elliptic and triangular flow of (anti)deuterons in Pb-Pb collisions at $\sqrt{s_{NN}} =$ 5.02 TeV, Phys. Rev. C **102**, 055203 (2020).

[5] A. Andronic, P. Braun-Munzinger, K. Redlich, and J. Stachel, Decoding the phase structure of QCD via particle production at high energy, Nature (London) **561**, 321 (2018).

[6] F. Bellini and A. P. Kalweit, Testing production scenarios for (anti-)(hyper-)nuclei and exotica at energies available at the CERN Large Hadron Collider, Phys. Rev. C **99**, 054905 (2019).

[7] S. T. Butler and C. A. Pearson, Deuterons from High-Energy Proton Bombardment of Matter, Phys. Rev. Lett. **7**, 69 (1961).

[8] H. Sato and K. Yazaki, On the coalescence model for high-energy nuclear reactions, Phys. Lett. B **98**, 153 (1981).

[9] R. Scheibl and U. W. Heinz, Coalescence and flow in ultrarelativistic heavy ion collisions, Phys. Rev. C **59**, 1585 (1999).

[10] K. Blum and M. Takimoto, Nuclear coalescence from correlation functions, Phys. Rev. C **99**, 044913 (2019).

[11] D. Oliinychenko, Overview of light nuclei production in relativistic heavy-ion collisions, Nucl. Phys. A **1005**, 121754 (2021).

[12] P. Danielewicz and G. F. Bertsch, Production of deuterons and pions in a transport model of energetic heavy ion reactions, Nucl. Phys. A **533**, 712 (1991).

[13] Y. Oh, Z.-W. Lin, and C. M. Ko, Deuteron production and elliptic flow in relativistic heavy ion collisions, Phys. Rev. C **80**, 064902 (2009).

[14] D. Oliinychenko, L.-G. Pang, H. Elfner, and V. Koch, Microscopic study of deuteron production in PbPb collisions at $\sqrt{s} = 2.76$ TeV via hydrodynamics and a hadronic afterburner, Phys. Rev. C **99**, 044907 (2019).

[15] D. Oliinychenko, L.-G. Pang, H. Elfner, and V. Koch, Centrality dependence of deuteron production in Pb+Pb collisions at 2.76 TeV via hydrodynamics and hadronic afterburner, MDPI Proc. **10**, 6 (2019).

[16] D. Oliinychenko, C. Shen, and V. Koch, Deuteron production in AuAu collisions at $\sqrt{s_{NN}} = 7$–200 GeV via pion catalysis, Phys. Rev. C **103**, 034913 (2021).

[17] V. Kireyeu, Cluster dynamics studied with the phase-space minimum spanning tree approach, Phys. Rev. C **103**, 054905 (2021).

[18] S. Gläßel, V. Kireyeu, V. Voronyuk, J. Aichelin, C. Blume, E. Bratkovskaya, G. Coci, V. Kolesnikov, and M. Winn, Cluster and hypercluster production in relativistic heavy-ion collisions within the parton-hadron-quantum-molecular-dynamics approach, Phys. Rev. C **105**, 014908 (2022).

[19] D. Everett *et al.* (JETSCAPE Collaboration), Phenomenological Constraints on the Transport Properties of QCD Matter with Data-Driven Model Averaging, Phys. Rev. Lett. **126**, 242301 (2021).

[20] D. Everett *et al.* (JETSCAPE Collaboration), Multisystem Bayesian constraints on the transport coefficients of QCD matter, Phys. Rev. C **103**, 054904 (2021).

[21] J. S. Moreland, J. E. Bernhard, and S. A. Bass, Alternative ansatz to wounded nucleon and binary collision scaling in high-energy nuclear collisions, Phys. Rev. C **92**, 011901(R) (2015).

[22] B. Schenke, S. Jeon, and C. Gale, (3+1)D hydrodynamic simulation of relativistic heavy-ion collisions, Phys. Rev. C **82**, 014903 (2010).

[23] B. Schenke, S. Jeon, and C. Gale, Elliptic and Triangular Flow in Event-by-Event (3+1)D Viscous Hydrodynamics, Phys. Rev. Lett. **106**, 042301 (2011).

[24] J.-F. Paquet, C. Shen, G. S. Denicol, M. Luzum, B. Schenke, S. Jeon, and C. Gale, Production of photons in relativistic heavy-ion collisions, Phys. Rev. C **93**, 044906 (2016).

[25] A. Bazavov *et al.* (HotQCD Collaboration), Equation of state in (2+1)-flavor QCD, Phys. Rev. D **90**, 094503 (2014).

[26] F. Cooper, G. Frye, and E. Schonberg, Landau's hydrodynamic model of particle production and electron positron annihilation into hadrons, Phys. Rev. D **11**, 192 (1975).

[27] J. Weil *et al.*, Particle production and equilibrium properties within a new hadron transport approach for heavy-ion collisions, Phys. Rev. C **94**, 054905 (2016).

[28] https://github.com/smash-transport/smash.

[29] D. Oliinychenko, V. Steinberg, J. Weil, M. Kretz, H. E. (Petersen), J. Staudenmaier, S. Ryu, A. Schäfer, J. Rothermel, J. Mohs, F. Li, L. Pang, D. Mitrovic, A. Goldschmidt, L. Geiger, L. Prinz, J.-B. Rose, and J. Hammelmann, smash-transport/smash: Smash-1.6 (2019), doi:10.5281/zenodo.3485108.

[30] M. Damodaran, D. Molnar, G. G. Barnaföldi, D. Berényi, and M. F. Nagy-Egri, Improved single-particle phase-space distributions for viscous fluid dynamic models of relativistic heavy ion collisions, Phys. Rev. C **102**, 014907 (2020).

[31] M. McNelis and U. Heinz, Modified equilibrium distributions for Cooper–Frye particlization, Phys. Rev. C **103**, 064903 (2021).

[32] D. Molnar and Z. Wolff, Self-consistent conversion of a viscous fluid to particles, Phys. Rev. C **95**, 024903 (2017).

[33] H. Grad, On the kinetic theory of rarefied gases, Commun. Pure Appl. Math. **2**, 331 (1949).

[34] B. Abelev *et al.* (ALICE Collaboration), Centrality dependence of π, K, p production in Pb-Pb collisions at $\sqrt{s_{NN}} = 2.76$ TeV, Phys. Rev. C **88**, 044910 (2013).

[35] K. Aamodt *et al.* (ALICE Collaboration), Centrality Dependence of the Charged-Particle Multiplicity Density at Midrapidity in Pb-Pb Collisions at $\sqrt{s_{NN}} = 2.76$ TeV, Phys. Rev. Lett. **106**, 032301 (2011).

[36] J. Adam *et al.* (ALICE Collaboration), Measurement of transverse energy at midrapidity in Pb-Pb collisions at $\sqrt{s_{NN}} = 2.76$ TeV, Phys. Rev. C **94**, 034903 (2016).

[37] K. Aamodt *et al.* (ALICE Collaboration), Higher Harmonic Anisotropic Flow Measurements of Charged Particles in Pb-Pb Collisions at $\sqrt{s_{NN}} = 2.76$ TeV, Phys. Rev. Lett. **107**, 032301 (2011).

[38] B. B. Abelev *et al.* (ALICE Collaboration), Event-by-event mean p_{T} fluctuations in pp and Pb-Pb collisions at the LHC, Eur. Phys. J. C **74**, 3077 (2014).

[39] B. I. Abelev *et al.* (STAR Collaboration), Systematic measurements of identified particle spectra in pp, d^+ Au and Au+Au Collisions from STAR, Phys. Rev. C **79**, 034909 (2009).

[40] J. Adams *et al.* (STAR Collaboration), Azimuthal anisotropy in Au+Au collisions at $\sqrt{s_{NN}} = 200$GeV, Phys. Rev. C **72**, 014904 (2005).

[41] L. Adamczyk *et al.* (STAR Collaboration), Third harmonic flow of charged particles in Au + Au collisions at $\sqrt{s_{NN}} = 200$ GeV, Phys. Rev. C **88**, 014904 (2013).

[42] J. Staudenmaier, D. Oliinychenko, J. M. Torres-Rincon, and H. Elfner, Deuteron production in relativistic heavy ion collisions via stochastic multiparticle reactions, Phys. Rev. C **104**, 034908 (2021).

[43] M. Kachelrieß, S. Ostapchenko, and J. Tjemsland, On nuclear coalescence in small interacting systems, Eur. Phys. J. A **57**, 167 (2021).

[44] J. E. Bernhard, J. S. Moreland, and S. A. Bass, Bayesian estimation of the specific shear and bulk viscosity of quark–gluon plasma, Nat. Phys. **15**, 1113 (2019).

[45] S. Acharya *et al.* (ALICE Collaboration), Production of charged pions, kaons, and (anti-)protons in Pb-Pb and inelastic *pp* collisions at $\sqrt{s_{NN}} = 5.02$ TeV, Phys. Rev. C **101**, 044907 (2020).
[46] J. Adam *et al.* (ALICE Collaboration), Centrality Dependence of the Charged-Particle Multiplicity Density at Midrapidity in Pb-Pb Collisions at $\sqrt{s_{NN}} = 5.02$ TeV, Phys. Rev. Lett. **116**, 222302 (2016).
[47] J. Adam *et al.* (ALICE Collaboration), Anisotropic Flow of Charged Particles in Pb-Pb Collisions at $\sqrt{s_{NN}} = 5.02$ TeV, Phys. Rev. Lett. **116**, 132302 (2016).
[48] A. Bilandzic, R. Snellings, and S. Voloshin, Flow analysis with cumulants: Direct calculations, Phys. Rev. C **83**, 044913 (2011).
[49] T. J. Santner, B. J. Williams, W. I. Notz, and B. J. Williams, *The Design and Analysis of Computer Experiments* (Springer, Berlin, 2003).
[50] H. Petersen, C. Coleman-Smith, S. A. Bass, and R. Wolpert, Constraining the initial state granularity with bulk observables in Au+Au collisions at $\sqrt{s_{\rm NN}} = 200$ GeV, J. Phys. G **38**, 045102 (2011).
[51] J. Novak, K. Novak, S. Pratt, J. Vredevoogd, C. E. Coleman-Smith, and R. L. Wolpert, Determining fundamental properties of matter created in ultrarelativistic heavy-ion collisions, Phys. Rev. C **89**, 034917 (2014).
[52] S. Pratt, E. Sangaline, P. Sorensen, and H. Wang, Constraining the Equation of State of Super-Hadronic Matter from Heavy-Ion Collisions, Phys. Rev. Lett. **114**, 202301 (2015).
[53] E. Sangaline and S. Pratt, Toward a deeper understanding of how experiments constrain the underlying physics of heavy-ion collisions, Phys. Rev. C **93**, 024908 (2016).
[54] J. E. Bernhard, J. S. Moreland, S. A. Bass, J. Liu, and U. Heinz, Applying Bayesian parameter estimation to relativistic heavy-ion collisions: Simultaneous characterization of the initial state and quark-gluon plasma medium, Phys. Rev. C **94**, 024907 (2016).
[55] J. E. Bernhard, P. W. Marcy, C. E. Coleman-Smith, S. Huzurbazar, R. L. Wolpert, and S. A. Bass, Quantifying properties of hot and dense QCD matter through systematic model-to-data comparison, Phys. Rev. C **91**, 054910 (2015).
[56] E. V. Bonilla, K. M. A. Chai, and C. K. I. Williams, Multi-task Gaussian process prediction, in *Proceedings of the 20th International Conference on Neural Information Processing Systems, NIPS'07* (Curran Associates, Red Hook, NY, 2007), p. 153–160.
[57] M. Byres, S. H. Lim, C. McGinn, J. Ouellette, and J. L. Nagle, Bulk viscosity and cavitation in heavy ion collisions, Phys. Rev. C **101**, 044902 (2020).
[58] F. S. Bemfica, M. M. Disconzi, V. Hoang, J. Noronha, and M. Radosz, Nonlinear Constraints on Relativistic Fluids Far from Equilibrium, Phys. Rev. Lett. **126**, 222301 (2021).
[59] C. Chiu and C. Shen, Exploring theoretical uncertainties in the hydrodynamic description of relativistic heavy-ion collisions, Phys. Rev. C **103**, 064901 (2021).
[60] C. Plumberg, D. Almaalol, T. Dore, J. Noronha, and J. Noronha-Hostler, Causality violations in realistic simulations of heavy-ion collisions, Phys. Rev. C **105**, L061901 (2022).
[61] http://www.tacc.utexas.edu.
[62] Ohio Supercomputer Center, http://osc.edu/ark:/19495/f5s1ph73, 1987.